Progress in Sputter Growth of β-Ga$_2$O$_3$ by Applying Pulsed-Mode Operation

Philipp Schurig, Fabian Michel, Andreas Beyer, Kerstin Volz, Martin Becker,* Angelika Polity, and Peter J. Klar

β-Ga$_2$O$_3$ thin films are deposited by pulsed radio-frequency (RF) magnetron sputtering on c-sapphire substrates, using a stoichiometric Ga$_2$O$_3$ target and a constant gas flux of an argon–oxygen mixture. Pulsed sputtering offers a way to overcome the restrictions of conventional sputtering. The parameters RF power and pulse duty cycle (PDC) are varied systematically to optimize the synthesis of Ga$_2$O$_3$ thin films. Subsequently, the resulting as-deposited (AD) Ga$_2$O$_3$ layers are analyzed in terms of structural and optical properties and the results are compared with those on the samples treated by postdeposition rapid thermal annealing. Based on this analysis, the process parameters are evaluated in terms of β-Ga$_2$O$_3$ formation. Postdeposition temperature treatments are found to yield a better crystal quality. However, a strong interdiffusion with the Al$_2$O$_3$ substrate is observed. The optical bandgap of the sputtered thin films is found to be quite independent of the RF sputtering power but to depend strongly on the PDC used, whereas the layer thickness rather strongly increases with both of those growth parameters. These evolutions are assigned to changes in the energy and ionic species of the plasma. Traces of GaO$_x$-related phases in addition to β-Ga$_2$O$_3$ are found in the interphase between the growing thin films and the underlying substrate.

1. Introduction

The quest for solar cell devices significantly contributing to satisfying the world's energy demand is on.[1–3] However, the only way to enable photovoltaics to fulfill the requirements of green

energy and overcome the limitations of resource criticality is to use semiconducting materials, which consist of chemical elements of high abundance. The different oxide phases of copper belong to this class of materials being sustainable and non-toxic. In particular, p-type cuprous oxide is of great interest, among others, as absorber materials in heterojunction solar cell devices in contact with n-type semiconductor window layers.[4–8] The term "window material" results from the fact that the radiation initially passes through this material virtually without interaction and is absorbed subsequently from the absorber layer. In addition to wide-band-gap nitride semiconductors such as GaN (3.4 eV)[9] and Al$_x$Ga$_{1-x}$N (3.4 − 3.75 eV)[10] or oxides such as ZnO (3.3 eV),[9] a material, very well suited for such devices as a window layer, might be gallium sesquioxide, Ga$_2$O$_3$. This material exhibits five different confirmed phases (α, β, γ, δ, and ε). Its polymorphism was first reported by Roy et al. as early as 1952.[11] Nowadays, research on this binary oxide is still very active, as there are a wide range of possible applications, especially for the thermodynamically most stable phase β-Ga$_2$O$_3$. In addition to the aforementioned heterojunction solar cell devices, the main reasearch topics include optoelectronic devices like light emitting diodes[12] and UV photodetectors,[13,14] electronic devices like field-effect transistors[15] and Schottky barrier diodes,[16–18] or devices for sensing gases[19,20] and radiation.[21,22] The prerequisite for the reliability and good performance of such devices is a reproducible material quality assured by standardized preparation procedures. For example, the electron concentration has to be controlled by defined synthesis conditions and postdeposition thermal annealing or doping. Native point defects in β-Ga$_2$O$_3$ are gallium vacancies, both on tetrahedral and octahedral lattice sites, and three different types of oxygen vacancies. However, residual impurities are needed to explain the electrical properties observed.[23] Doping with elements like Si, Ge, and Sn on Ga sites or F on oxygen sites is feasible to establish n-type conduction.[24–26] Due to the intensive research particularly in the context of power devices, several review articles have emerged on gallium oxides and their properties.[27–32]

Synthesis of bulk Ga$_2$O$_3$ is well established. By far the largest number of publications deal with β-Ga$_2$O$_3$ and certain aspects of its versatility. Crystals of a high structural quality are available.

P. Schurig, F. Michel, Dr. M. Becker, Dr. A. Polity, Prof. P. J. Klar
Institute for Experimental Physics I and Center for Materials Research (LaMa)
Justus Liebig University Giessen
Heinrich-Buff-Ring 16, 35392 Giessen, Germany
E-mail: martin.becker@exp1.physik.uni-giessen.de

Dr. A. Beyer, Prof. K. Volz
Institute of Physical Chemistry and Materials Science Center
Philipps-University Marburg
Hans-Meerwein-Straße 6, 35032 Marburg, Germany

ADVANCED
SCIENCE NEWS
www.advancedsciencenews.com

physica
pss
status solidi
a

www.pss-a.com

They can be produced by gas phase and flux growth techniques, as well as melt growth methods, which present a main technological advantage compared with other wide-bandgap materials of industrial importance, i.e., gallium nitride and silicon carbide. Although different kinds of bulk growth techniques in different environments exist, nowadays, melt growth techniques dominate due to the industrial applicability on large scale.[31,32] Demonstrably, the Czochralski method,[33,34] edge-defined film-fed growth (EFG),[35] and vertical Bridgman (VB) methods[36] are capable of fulfilling the need of upscaling. For example, EFG can be used to produce even 4 inch-diameter single-crystal wafers.[37] Thin films can be realized by a variety of techniques, chemical vapor deposition (CVD),[38–41] metal-organic chemical vapor deposition (MOCVD),[42] molecular beam epitaxy (MBE),[43–48] pulsed laser deposition (PLD),[5,49–51] and sol–gel synthesis,[52–55] among others. A topical review with focus on the progress in the synthesis of bulk as well as thin films of Ga_2O_3 was recently given by Galazka.[32]

As growth conditions or postgrowth annealing parameters influence layer properties like degree of crystallinity, composition, or morphology, among others, each deposition method has its own right to exist depending on the application sought for. The main objective, however, is to bring in line the material properties with economic and financial efficiency. Therefore, an increase in the growth rate is often required to ensure use on an industrial scale. In those cases, sputtering techniques seem to be viable candidates for achieving this goal.[56,57] Atoms ejected from the target's surface by energetic ion impingement are neutral unless they are ionized, inter alia, by application of very high power to the discharge.[58] The target power density, however, is limited owing to target heating. Hence, obtaining thin layers of an insulating material with low defect densities and high compactness is very challenging. The process is mainly hampered by the occurrence of arc events at the target, however, pulsing the magnetron discharge has been found to stabilize the reactive sputtering process. In pulsed DC deposition systems glow discharges with a target power density of up to $900\,W\,cm^{-2}$ have been obtained.[59] Thus, switching from standard to the pulsed mode at constant target power is promising to overcome the main challenge in obtaining crystalline β-Ga_2O_3, namely acquiring the secondary particle energy necessary for growth along a preferential crystal orientation. However, literature concerning the influence of the additional sputter parameters, e.g. pulse duty cycle (PDC) or pulse repetition frequency (PRF), on metal oxide growth is still scarce.

In this work, we discuss the sputter deposition of Ga_2O_3 thin films on c-sapphire substrates using radio-frequency (RF) magnetron sputtering in the pulsed mode and compare the layers obtained with thin films deposited by conventional RF magnetron sputtering. Sputtering power as well as PDC was varied. Additionally, the influence of a postdeposition thermal annealing step is investigated. Subsequently, the Ga_2O_3 films were analyzed to identify a suitable growth window for β-Ga_2O_3.

2. Experimental Section

Ga_2O_3 thin films were grown on c-plane sapphire substrates by conventional RF magnetron sputtering at 13.56 MHz. The substrates were cleaned with acetone and methanol in an ultrasonic bath, dried with nitrogen, and mounted in the sputter chamber (base pressure of 5×10^{-7} mbar) subsequently. In the growth process, a plasma of the process gas was generated between the target and the substrate. Ions of the process gas, in our case, a mixture of inert argon and reactive molecular oxygen (ratio 4:1), impinged onto a target, here, a Ga_2O_3 ceramic target and sputter-off target atoms. These atoms along with the reactive species of the process gas formed an oxide film on the substrate. The RF power coupled into the plasma was generated by a "Dressler CESAR 1312" system equipped with a "Dressler VM 1500 AW" matching network. Additionally, the regular sputtering mode of the very same RF power generator was superimposed by a selected frequency scheme. Utilizing this mode of operation additional parameters may be varied. Most importantly, the PDC, the on-to-off ratio of sputter time, was changed between 10% and 70%.

The growth temperature was kept constant at 650 K based on measuring the temperature with a thermocouple. The temperature, the actual growth temperature (surface temperature), was expected to be considerably higher, depending on the RF power coupled into the plasma, the target-substrate geometry, and the target's thermal conductivity. The temperature range was chosen in accordance with the findings of Akazawa and Zhang et al., who observed the threshold temperature of crystalline Ga_2O_3 at 500 and 300 °C, respectively.[56,60] Details on the distinct temperature characteristics of the setup can be found elsewhere.[57]

Here, we discuss two series of samples. Throughout each series a specific process parameter was varied systematically, whereas all the other process parameters were kept constant, cf. **Table 1**. The variables chosen were RF sputter power in series I and PDC in series II. Thus, series I resembled conventional RF sputter deposition at fixed PRF and PDC values, whereas series II illustrated the impact of using the pulsed mode in the sputter deposition of β-Ga_2O_3. The results of the series were compared with measurements conducted on samples which were conventionally sputtered using the same setup and reported previously.[57] All samples were unintentionally doped and, thus, did not show significant electrical conductivity, which was most likely driven by the pronounced grain structure intrinsic for sputtered thin films.

After all as-deposited (AD) samples were measured, and a rapid thermal annealing process was conducted on all specimens. The samples were treated at 1000 °C for 1 h in ambient atmosphere. All as-grown Ga_2O_3 films as well as all annealed specimens were analyzed by X-ray diffraction (Siemens D 5000) in a Bragg–Brentano $\Theta-2\Theta$ geometry. Optical transmittance at normal incidence ($\beta = 0°$) and relative specular reflectance close to normal incidence ($\beta = 6°$) were recorded using a "PerkinElmer Lambda 900" spectrometer. The influence of the substrate was eliminated by measuring a substrate baseline prior to thin-film deposition. The morphology of the sample surfaces

Table 1. Parameters used in the pulsed sputter processes for depositing sample series I and II.

Series	RF power [W]	PDC [%]	PRF [kHz]	Plasma on-time [min]
I	600–1000	10	1	6
II	800	10–70	1	6

ADVANCED
SCIENCE NEWS
www.advancedsciencenews.com

physica
status
solidi a

www.pss-a.com

was studied by scanning electron microscopy (SEM) and atomic force microscopy (AFM), using a Zeiss MERLIN scanning electron microscope equipped with an In-Lens detector and an AIST-NT SmartSPM operating in the noncontact mode. Raman spectra with a spectral resolution of 1.5 cm^{-1} were acquired with a Renishaw inVia Raman microscope system using 514 nm laser excitation. Electron-transparent samples were prepared using a JEOL JIB-4601F dual beam system operating at 3−30 kV. Thin protective layers of carbon and tungsten were deposited by the electron beam-assisted deposition on the surface of the thin film. This was followed by 2 μm thick carbon and tungsten layer deposition using the Ga ion beam. This procedure was chosen to not damage the surface with impinging Ga ions during initial growth. A cross-sectional sample was produced by thinning down the sample from the substrate side to 500 nm with a 30 kV ion beam and then to 300 and 200 nm using a 15 and 10 kV ion beam, respectively. Finally, the material was thinned to about 100 nm with 5 kV ions and polishing was done with a 3 kV ion beam to remove the damaged layer. Transmission electron microscopy (TEM) characterization, i.e. the acquisition of high-resolution images as well as selected-area electron diffraction (SAED) patterns, was conducted in a JEOL JEM 3010 operating at 300 kV.

3. Results and Discussion

First, we will recap tendencies observed in the conventional RF sputter deposition of Ga$_2$O$_3$.[57] The optical bandgap strongly depends on the deposition parameters oxygen flux, heating power, and RF power. Polycrystalline β-Ga$_2$O$_3$ with an optical bandgap and a refractive index close to the values of bulk material was obtained under oxygen excess at a low RF power and relatively moderate growth temperatures of about 600 °C. The general trend of the optical bandgaps depending on RF sputtering power is explained as follows. Less kinetic energy of the process gas ions impinging on the target results from a lower RF power coupled

into the plasma. Excess oxygen is required to compensate the excess of Ga due to preferential sputtering in the particle flux toward the substrate.[61] In summary, at the fixed gas flux ratio, increasing the RF power was found to influence the optical parameters the most. An increase in growth temperature resulted in an enhanced crystal quality and a composition tending toward stoichiometry. Unfortunately, the conventional RF magnetron sputter setup is limited in further increasing heating power and lowering RF power and, thus, achieving higher crystallinity.

A common way to overcome this drawback is to perform post-deposition temperature treatment. Crystallinity might be enhanced by heating the films, as atoms on the lattice may rearrange and oxygen vacancies or interstitials may be removed, depending on the surrounding atmosphere. However, we found that in the case of heterostructures of Ga$_2$O$_3$ and Al$_2$O$_3$ (sapphire), strong interdiffusion occurs at the high annealing temperatures of about 1000 °C. We found by secondary-ion mass spectrometry measurements that after annealing for 1 h, the Al content in the Ga$_2$O$_3$ films is increased by almost two orders of magnitude, corresponding to atomic fractions in the order of percent, cf. Supporting Information.

Thus, an alternative way has to be sought for improving the layer quality. To circumvent the restrictions of the conventional continuous sputtering process, we switch to a pulsed operation. In doing so, the sputtering power might be further enhanced to effectively yield higher growth temperatures. Similar to conventional RF sputtering the increase in applied RF power should enhance the primary particle energy and, thus, the particles' ability to sputter target atoms. Consequently, it is assumed that the grown oxide layers are thicker and of enhanced crystallinity.

Figure 1 shows the results for series I, in which the RF sputtering power was varied for fixed PRF and PDC values of 1 kHz and 10%, respectively. The layer thicknesses linearly increase with the RF sputtering power from 300 to 700 nm, cf. Figure 1a. However, they do not change much after annealing. The error margins shown originate from the uncertainty of the refractive index value used in thickness determination.[43] The layer
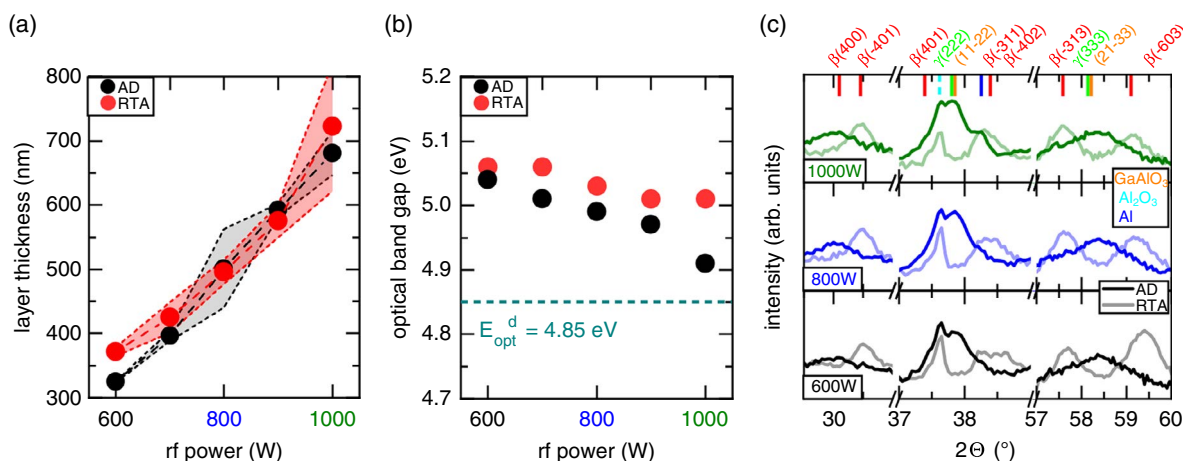

Figure 1. a) Layer thickness and b) optical bandgap of AD and rapid thermal annealed (RTA) Ga$_2$O$_3$ layers deposited on c-plane sapphire by varying the pulsed RF sputtering power. Error margins given in (a) arise due to the uncertainty of the refractive index used in the analysis.[43] While the layer thickness is not affected significantly by the thermal annealing procedure, the optical bandgaps exceed in this sputter series, most likely due to the Al interdiffusion. c) X-ray diffractograms for selected samples, deposited at 600, 800 and 1000 W, respectively. Although there is no significant influence of the RF power for AD samples, slight changes in the reflection ratios might be detected for the annealed samples.

ADVANCED
SCIENCE NEWS
www.advancedsciencenews.com

physica
status
solidi a
www.pss-a.com

thicknesses obtained translate to growth rates of around 50–120 nm min^{-1} plasma on-time. Compared with the growth rate of approximately 4–5 nm min^{-1} found for conventionally sputtered layers,[57] this is a significant improvement.

The optical bandgaps of the samples of series I are shown in Figure 1b. The samples grown at the highest RF power exhibit optical bandgaps closest to values reported for stoichiometric β-Ga$_2$O$_3$.[62,63] At first glance, this seems contradictory to what was obtained for conventionally sputtered samples, where the lowest RF power yielded optical bandgaps closest to the theoretical value for stoichiometric β-Ga$_2$O$_3$.[57] However, the general trend of the optial bandgap values of Ga$_2$O$_3$ with increasing RF sputtering power is the same, as they significantly decrease in a linear fashion from 5.1 to 4.9 eV. Thus, we tentatively assign the cause of the findings in Figure 1b to be a superposition of two effects: first, the effect of RF sputter power on the preferential sputtering being the same, as shown for conventional sputtering, and the overall shift of this tendency to higher bandgaps triggered by the pulsed operation. Thus, a careful tuning of RF sputtering power and oxygen flux being intertwined is necessary to yield bulk material's optical bandgap.

After rapid thermal annealing the optical bandgaps obtained for the Ga$_2$O$_3$ layers increased compared with those of the AD samples. We ascribe this enhancement to the diffusion of Al from the sapphire substrate into the Ga$_2$O$_3$ layer. Thus, metastable phases like (Ga,Al)O$_3$ might be present in the polycrystalline structure. Additionally, there seems to be a saturation at optical bandgaps of around 5.0 eV for the annealed samples. As Al and Ga are chemically similar, it is possible to substitute either easily by the other.[64,65] However, with increasing sputtering power, which translates to a larger layer thickness, this effect slowly becomes less important as the layer thickness exceeds the maximum diffusion length of Al in Ga$_2$O$_3$ at 1000 °C reached after 1 h.

Figure 1c shows X-ray diffractograms for selected samples, deposited at 600, 800, and 1000 W, respectively, in the AD state (bold) as well as after postdeposition thermal treatment (transparent). The AD layers exhibit broad peaks of low intensities at about 30°, 38°, and 58.5°, which may be assigned to the reflections (400), (−313), and (−603) β-Ga$_2$O$_3$, although being shifted compared with the literature values of bulk material. However, a trustworthy assignment is rather difficult, as reflections of other gallium oxide phases like γ-Ga$_2$O$_3$ or even metastable phases like (Ga,Al)O$_3$ might be superimposed.

In principle, α-phase Ga$_2$O$_3$ shows a better lattice match with c-plane sapphire than its β-phase. However, β-phase Ga$_2$O$_3$ is more commonly observed when growth occurs on this kind of substrate, presumably due to its lower chemical potential.[56,57] Furthermore, surface roughness and defect density on the substrate surface affect the growth conditions and, thus, the crystallization of different phases.[56,60,66] For example, a shift from β-phase to γ-phase was observed when growing in an environment containing water vapor, detrimental for the formation of high-temperature phases.[56] Thus, we expect the diffractogram to change significantly after carrying out postgrowth thermal treatment. Indeed, after annealing the reflections shift significantly or even vanish completely. While the untreated layers are mainly amorphous, at least what can be deduced from X-ray diffraction, with exception of broad peaks not to

be assigned to a distinct plane or phase, annealed samples show different out-of-plane orientations of the β-phase and may be considered polycrystalline. In particular, the (−401) and (−313) reflections of β-Ga$_2$O$_3$ appear, whereas reflections of the {−h01} family of planes shift toward the value of bulk material. This is in line with the findings of Roy et al. that gallium oxide transforms into the β-phase at elevated temperatures, no matter which phase had been present beforehand.[11] Another hint can be found when comparing the samples grown in the pulsed mode with those sputtered in the non-pulsed fashion. While the former shows reflections presumably corresponding to a superposition of various phases, the latter clearly exhibits β-Ga$_2$O$_3$, although slightly strained.[57]

Thus, we suspect pulsed-mode sputtering to support the synthesis of mixed-phase samples which then vanish under postgrowth thermal treatment. Especially the rather strong contributions of reflections, tentatively assigned to γ-Ga$_2$O$_3$, disappear. Similar to the α-phase the thermodynamic stability of the γ-phase is only metastable and changes into the β-phase above 650 °C.[11]

Series II was deposited at different PDCs, cf. Table 1, to clarify its impact on the thin-film growth. A PDC of 100% corresponds to conventional RF sputter deposition. Thus, increasing the PDC leads to prolonged sputter pulses and thus to higher plasma on-times. To detach an influence of the PDC itself from an influence of increased plasma on-times, the total plasma on-time was kept constant by reducing the overall sputter time.

Figure 2a shows the dependence of layer thickness as a function of the PDC. The values obtained increase nonlinearly between 0.5 and 2.6 μm with the highest slope in the intermediate range between 40% and 50% PDC. We tentatively assign this evolution to changes in the energy and species of the plasma ions. Keeping the RF sputtering power constant, the increase in PDC is synonymous with the increase in on-time in which the ions are accelerated. As a consequence, changing the PDC value will affect the energy distribution, species, and cross sections of dominant primary ions and, as a consequence, the properties of the secondary target particles can be manipulated.[67] Thus, inter alia, the timescale for ordering at the substrate surface is modified. Sputtered species may have gained enough energy to statistically evaporate after arriving at the substrate surface, resulting in a saturation behavior of the remaining layer thickness. Additionally, it is known that pulsed-mode sputtering increases the rate of negatively charged oxygen atoms, which may impinge on the surface of the growing layer and induce surface etching, resulting in reduced layer thickness. Analysis of the distribution of plasma species and their impact on the overall process is ongoing.

The corresponding optical bandgaps versus PDC are shown in Figure 2b. With increasing PDC value the optical bandgaps decrease until they reach values around 4.65 eV. Below the optical bandgap of bulk β-Ga$_2$O$_3$ the decrease might be explained by an increased defect density caused by less time for the atomic species to a suitable order on the substrate surface at high PDC. Accordingly, for a given frequency, the PDC value has to be optimized for a given sputtering power.

It should be noted that the annealing process has very limited influence on both the layer thickness and the optical bandgaps. If any, there is a deviation of the optical bandgaps of layers
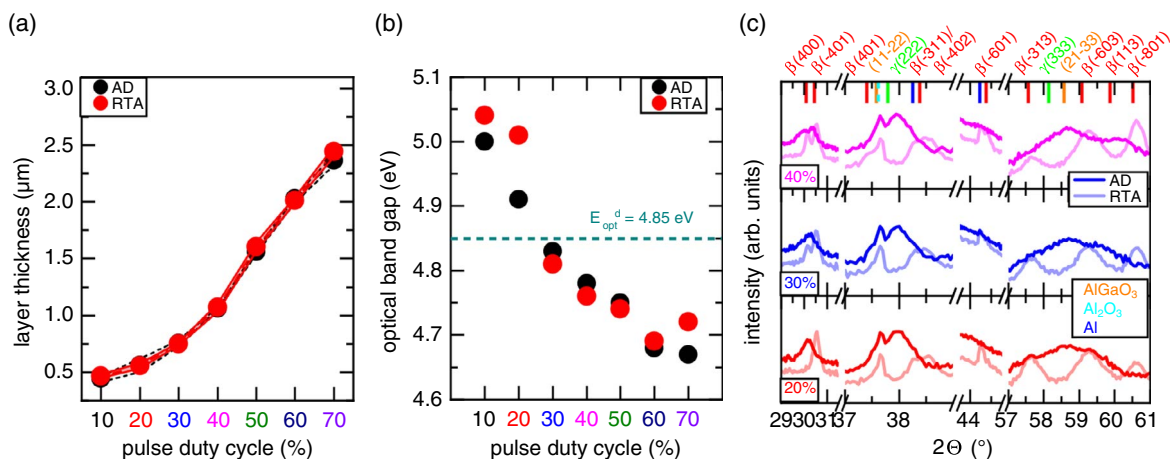
Figure 2. a) Layer thickness and b) optical bandgap of the AD and RTA Ga_2O_3 layers deposited on c-plane sapphire by varying the PDC. Error margins given in (a) arise due to the uncertainty of the refractive index used in the analysis.[43] c) X-ray diffractograms for selected samples, deposited at 20%, 30%, and 40% PDC, respectively.

grown at low PDCs. Here, the higher bandgaps of annealed samples might again well be attributed to Al diffusion into the Ga_2O_3, as this effect is known to be more significant for thinner samples. One might even think of alloying in the vicinity of the substrate, resulting in the $GaAlO_3$ spinel. More insight into this is given by the structural analysis. In this context, Figure 2c shows the diffractogram of the layers deposited at 20%, 30%, and 40% PDC, respectively. The AD layers are shown in bold colors and the thermally treated samples in transparent colors. Comparing the data with the diffractograms shown in Figure 1c, no significant changes can be observed. So the general trend of pulsed-mode sputtering to support the synthesis of mixed-phase samples which then vanish under postgrowth thermal treatment still holds. Thus, the broad reflections at 38° and 58.5° most likely represent the (222) and (333) reflection of γ-Ga_2O_3. Due to the overall low crystalline quality, however, one has to assume rather small γ-Ga_2O_3 domains in an amorphous matrix. After thermal annealing the γ-Ga_2O_3 peaks vanish due to phase transformation to the β-phase, taking place above 650 °C. Thus, all reflections observed in the annealed layers may be interpreted as β-Ga_2O_3, confirming better crystalline quality. However, there also exist minor differences compared with the results shown in Figure 1c. One such difference is the appearance of additional or at least more pronounced reflections for the annealed samples around 30°, 44°, and 60.5°. All these reflections belong to the $\{-h01\}$ family of planes and increase in relative intensity when the PDC is increased. It seems that the $\{-h01\}$ family of planes exhibits a comparatively high formation energy, which is delivered only at higher duty cycles.

To further evaluate the actual crystallinity of a representative pulsed sputtered Ga_2O_3 thin film, we will now focus on the sample grown at 800 W RF sputter power and 30% PDC. **Figure 3** shows a) the corresponding Raman spectra of the annealed layer in comparison with those of an untreated layer and a sapphire substrate as references, as well as the surface morphology of the annealed and as-grown Ga_2O_3 samples measured by b) SEM and c) AFM. Although it is beyond this article to evaluate the data in

detail, both Raman spectra and the surface morphology investigated via SEM and AFM, respectively, confirm a more pronounced crystallinity after annealing.[68] Especially Raman spectroscopy is known to very sensitively differentiate material phases[48,69,70] or locate defect structures.[71] Thus, the presumption of the conversion of amorphous material into β-Ga_2O_3 throughout the discussion is further underlined.

Additionally, TEM measurements were carried out, cf. Figure 3d–f, especially to investigate the interface region between the Ga_2O_3 layer and the Al_2O_3 substrate. Figure 3d shows the SAED pattern obtained from a thin slice of a thin film deposited at 30% PDC. The circles in the pattern indicate polycrystalline material.[72] Therefore, the SAED pattern underlines the findings of the XRD measurement in that polycrystalline domains in an amorphous matrix are present. A cross-sectional TEM view, cf. Figure 3e, enables a distinction between the polycrystalline and amorphous domains and even differently oriented domains. However, the most striking feature is the possibility to investigate the interface region, cf. Figure 3f. It should be noted that the interface appears to be smeared out, indicating slight interdiffusion. As the measurements shown represent an as-grown sample, this is most likely an effect of the impingment of negatively charged oxygen ions.[73] Nevertheless, the structure of the substrate continues for some nm in the Ga_2O_3 layer, replacing Al atoms by Ga atoms (a brighter impression). Thus, we tentatively assign this pseudomorphous grown region as γ-Ga_2O_3.

It should be noted that α-Ga_2O_3 might also be observed at the interface with sapphire.[74,75] Phase stabilization of α-Ga_2O_3 was observed on r-plane α-Al_2O_3 in plasma-assisted MBE up to a film thickness of around 200 nm.[76] Thus, initially the resulting strain energy due to lattice mismatch shifts the thermodynamic equilibrium from the stable β-Ga_2O_3 toward the metastable α-modification.[77] However, for increasing growth times, nucleation of β-phase was found on the c-plane facets of α-Ga_2O_3. Here, we do not see any indication of the α-phase being present in the interface, although we cannot rule out entirely the presence of some domains.
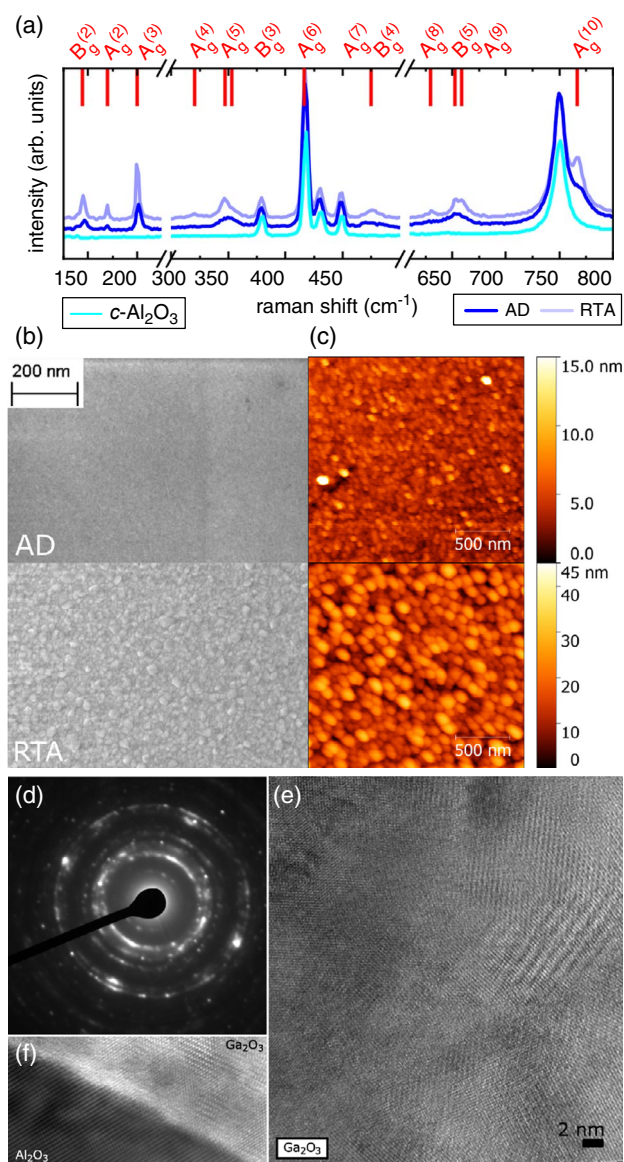
Figure 3. (a) Raman spectra of a representative pulsed-sputtered Ga_2O_3 thin film, grown at 800 W RF sputter power and 30% PDC. The theoretical mode positions displayed earlier were taken from Kranert et al.[78] b) SEM and c) AFM measurements of annealed samples in comparison with an as-deposited layer. An increase in temperature is accompanied by an increased amount of crystalline phase. d) SAED pattern, e) cross-sectional TEM, and f) HRTEM measurement of the interface region between the Ga_2O_3 layer and the Al_2O_3 substrate for the AD sample grown at 800 W RF sputter power and 30% PDC.

4. Conclusions

Thin films of β-Ga_2O_3 were deposited by pulsed RF magnetron sputtering on c-sapphire substrates. The growth rates were significantly increased compared with those measured for conventionally sputtered β-Ga_2O_3 layers. The optical bandgap of the sputtered thin films was found to be quite independent of the RF sputtering power but to depend strongly on the PDC, whereas the layer thickness rather strongly increased with both of those growth parameters. We tentatively assign these evolution to changes in the energy and species of the plasma ions. However, the overall crystal quality of β-Ga_2O_3 is still in need of improvement, which we assign to the presence of other GaO_x-related phases at the interphase between β-Ga_2O_3 and the underlying substrate.

Conflict of Interest

The authors declare no conflict of interest.

[1] A. Feltrin, A. Freundlich, *Renew. Energy* **2008**, *33*, 180.
[2] C. Wadia, A. P. Alivisatos, D. M. Kammen, *Environ. Sci. Technol.* **2009**, *43*, 2072.
[3] T. Unold, H. W. Schock, *Annu. Rev. Mater. Res.* **2011**, *41*, 297.
[4] B. K. Meyer, A. Polity, D. Reppin, M. Becker, P. Hering, P. J. Klar, T. Sander, C. Reindl, J. Benz, M. Eickhoff, C. Heiliger, M. Heinemann, J. Bläsing, A. Krost, S. Shokovets, C. Müller, C. Ronning, *Phys. Status Solidi B* **2012**, *249*, 1487.
[5] T. Minami, Y. Nishi, T. Miyata, *Appl. Phys. Express* **2013**, *6*, 044101.
[6] T. Minami, Y. Nishi, T. Miyata, *Appl. Phys. Express* **2015**, *8*, 022301.
[7] T. Minami, Y. Nishi, T. Miyata, *Appl. Phys. Express* **2016**, *9*, 052301.
[8] Y. S. Lee, D. Chua, R. E. Brandt, S. C. Siah, J. V. Li, J. P. Mailoa, S. W. Lee, R. G. Gordon, T. Buonassissi, *Adv. Mater.* **2014**, *26*, 4704.
[9] B. Kramm, A. Laufer, D. Reppin, A. Kronenberger, P. Hering, A. Polity, B. K. Meyer, *Appl. Phys. Lett.* **2012**, *100*, 094102.
[10] F. Michel, B. Kramm, M. Becker, K. P. Hering, D. M. Hofmann, P. J. Klar, *J. Appl. Phys.* **2018**, *123*, 245304.
[11] R. Roy, V. G. Hill, E. F. Osborn, *J. Am. Chem. Soc.* **1952**, *74*, 719.
[12] D. Li, V. Hoffmann, E. Richter, T. Tessaro, Z. Galazka, M. Weyers, G. Tränkle, *J. Cryst. Growth* **2017**, *478*, 212.
[13] T. Ohshima, T. Okuno, N. Arai, N. Suzuki, S. Ohira, S. Fujita, *Appl. Phys. Express* **2008**, *1*, 011202.
[14] M. Zhong, Z. Wei, X. Meng, F. Wu, J. Li, *J. Alloy. Compd.* **2015**, *619*, 572.
[15] M. Higashiwaki, K. Sasaki, A. Kuramata, T. Masui, S. Yamakoshi, *Appl. Phys. Lett.* **2012**, *100*, 013504.

[16] D. Splith, S. Müller, F. Schmidt, H. von Wenckstern, J. J. van Rensburg, W. E. Meyer, M. Grundmann, *Phys. Status Solidi A* **2014**, *211*, 40.

[17] S. Müller, H. von Wenckstern, F. Schmidt, D. Splith, F. L. Schein, H. Frenzel, M. Grundmann, *Appl. Phys. Express* **2015**, *8*, 121102.

[18] Q. He, W. Mu, H. Dong, S. Long, Z. Jia, H. Lv, Q. Liu, M. Tang, X. Tao, M. Liu, *Appl. Phys. Lett.* **2017**, *110*, 093503.

[19] M. Bartic, M. Ogita, M. Isai, C. Baban, H. Suzuki, *J. Appl. Phys.* **2007**, *102*, 023709.

[20] R. Pandeeswari, B. G. Jeyaprakash, *Sens. Actuators B* **2014**, *195*, 206.

[21] Y. Usui, T. Oya, G. Okada, N. Kawaguchi, T. Yanagida, *Optik* **2017**, *143*, 150.

[22] Y. Usui, D. Nakauchi, N. Kawano, G. Okada, N. Kawaguchi, T. Yanagida, *J. Phys. Chem. Solids* **2018**, *117*, 36.

[23] J. B. Varley, H. Peelaers, A. Janotti, C. G. Van de Walle, *J. Phys.: Condens. Matter* **2011**, *23*, 334212.

[24] M. Higashiwaki, K. Sasaki, T. Kamimura, M. H. Wong, D. Krishnamurthy, A. Kuramata, T. Masui, S. Yamakoshi, *Appl. Phys. Lett.* **2013**, *103*, 1.

[25] A. J. Green, K. D. Chabak, E. R. Heller, R. C. Fitch, M. Baldini, A. Fiedler, K. Irmscher, G. Wagner, Z. Galazka, S. E. Tetlak, A. Crespo, K. Leedy, G. H. Jessen, *IEEE Electron Device Lett.* **2016**, *37*, 902.

[26] E. G. Villora, K. Shimamura, Y. Yoshikawa, T. Ujiie, K. Aoki, *Appl. Phys. Lett.* **2008**, *92*, 174.

[27] M. Higashiwaki, H. Murakami, Y. Kumagai, A. Kuramata, *Jpn. J. Appl. Phys.* **2016**, *55*, 1202A1.

[28] S. I. Stepanov, V. I. Nikolaev, V. E. Bougrov, A. E. Romanov, *Rev. Adva. Mater. Sci.* **2016**, *44*, 63.

[29] H. v. Wenckstern, *Adv. Electron. Mater.* **2017**, *3*, 1600350.

[30] M. A. Mastro, A. Kuramata, J. Calkins, J. Kim, F. Ren, S. J. Pearton, *ECS J. Solid State Sci. Technol.* **2017**, *6*, P356.

[31] M. Baldini, Z. Galazka, G. Wagner, *Mater. Sci. Semicond. Proc.* **2018**, *78*, 132.

[32] Z. Galazka, *Semicond. Sci. Technol.* **2018**, *33*, 113001.

[33] Z. Galazka, K. Irmscher, R. Uecker, R. Bertram, M. Pietsch, A. Kwasniewski, M. Naumann, T. Schulz, R. Schewski, D. Klimm, M. Bickermann, *J. Cryst. Growth* **2014**, *404*, 184.

[34] Z. Galazka, R. Uecker, D. Klimm, K. Irmscher, M. Naumann, M. Pietsch, A. Kwasniewski, R. Bertram, S. Ganschow, M. Bickermann, *ECS J. Solid State Sci. Technol.* **2017**, *6*, Q3007.

[35] A. Kuramata, K. Koshi, S. Watanabe, Y. Yamaoka, T. Masui, S. Yamakoshi, *Jpn. J. Appl. Phys.* **2016**, *55*, 1202A2.

[36] K. Hoshikawa, E. Ohba, T. Kobayashi, J. Yanagisawa, C. Miyagawa, Y. Nakamura, *J. Cryst. Growth* **2016**, *447*, 36.

[37] H. Aida, K. Nishiguchi, H. Takeda, N. Aota, K. Sunakawa, Y. Yaguchi, *Jpn. J. Appl. Phys.* **2008**, *47*, 8506.

[38] G. A. Battiston, R. Gerbasi, M. Porchia, R. Bertoncello, F. Caccavale, *Thin Solid Films* **1996**, *279*, 115.

[39] E. Auer, A. Lugstein, S. Löffler, Y. J. Hyun, W. Brezna, E. Bertagnolli, P. Pongratz, *Nanotechnology* **2009**, *20*, 434017.

[40] T. Terasako, H. Ichinotani, M. Yagi, *Phys. Status Solidi C* **2015**, *12*, 985.

[41] S. Rafique, L. Han, H. Zhao, *Phys. Status Solidi A* **2016**, *213*, 1002.

[42] N. M. Sbrockey, T. Salagaj, E. Coleman, G. S. Tompa, Y. Moon, M. S. Kim, *J. Electron. Mater.* **2015**, *44*, 1357.

[43] M. Rebien, W. Henrion, M. Hong, J. P. Mannaerts, M. Fleischer, *Appl. Phys. Lett.* **2002**, *81*, 250.

[44] E. G. Villora, K. Shimamura, K. Kitamura, K. Aoki, *Appl. Phys. Lett.* **2006**, *88*, 031105.

[45] K. Sasaki, A. Kuramata, T. Masui, E. G. Villora, K. Shimamura, S. Yamakoshi, *Appl. Phys. Express* **2012**, *5*, 035502.

[46] H. Okumura, M. Kita, K. Sasaki, A. Kuramata, M. Higashiwaki, J. S. Speck, *Appl. Phys. Express* **2014**, *7*, 095501.

[47] P. Vogt, O. Bierwagen, *Appl. Phys. Lett.* **2016**, *109*, 062103.

[48] M. Kracht, A. Karg, J. Schörmann, M. Weinhold, D. Zink, F. Michel, M. Rohnke, M. Schowalter, B. Gerken, A. Rosenauer, P. J. Klar, J. Janek, M. Eickhoff, *Phys. Rev. Appl.* **2017**, *8*, 054002.

[49] M. Orita, H. Ohta, M. Hirano, H. Hosono, *Appl. Phys. Lett.* **2000**, *77*, 4166.

[50] M. Orita, H. Hiramatsu, H. Ohta, M. Hirano, H. Hosono, *Thin Solid Films* **2002**, *411*, 134.

[51] K. Matsuzaki, H. Hiramatsu, K. Nomura, H. Yanagi, T. Kamiya, M. Hirano, H. Hosono, *Thin Solid Films* **2006**, *496*, 37.

[52] T. Minami, *Solid-State Electron.* **2003**, *47*, 2237.

[53] Y. Li, A. Trinchi, W. Wlodarski, K. Galatsis, K. K. Zadeh, *Sens. Actuators B* **2003**, *93*, 431.

[54] Y. Kokubun, K. Miura, F. Endo, S. Nakagomi, *Appl. Phys. Lett.* **2007**, *90*, 031912.

[55] R. Moos, N. Izu, F. Rettig, S. Reiss, W. Shin, I. Matsubara, *Sensors* **2011**, *11*, 3439.

[56] H. Akazawa, *Vacuum* **2016**, *123*, 8.

[57] P. Schurig, M. Couturier, M. Becker, A. Polity, P. J. Klar, *Phys. Status Solidi A* **2019**, 1900385.

[58] W. M. Posadowski, *Vacuum* **1995**, *46*, 1017.

[59] R. Gruen, US Patent 5 015 493, (**1991**).

[60] F. B. Zhang, K. Saito, T. Tanaka, M. Nishio, Q. X. Guo, *J. Cryst. Growth* **2014**, *387*, 96.

[61] S. S. Kumar, E. J. Rubio, M. Noor-A-Alam, G. Martinez, S. Manandhar, V. Shutthanandan, *J. Phys. Chem.* **2013**, *177*, 4194.

[62] J. B. Varley, J. R. Weber, A. Janotti, C. G. Van de Walle, *Appl. Phys. Lett.* **2010**, *97*, 142106.

[63] C. Janowitz, V. Scherer, M. Mohamed, A. Krapf, H. Dwelk, R. Manzke, Z. Galazka, R. Uecker, K. Irmscher, R. Fornari, M. Michling, D. Schmeißer, J. R. Weber, J. B. Varley, C. G Van de Walle, *New J. Phys.* **2011**, *13*, 085014.

[64] V. G. Hill, R. Roy, E. F. Osborn, *J. Am. Ceram. Soc.* **1952**, *35*, 135.

[65] T. Oshima, T. Okuno, N. Arai, Y. Kobayashi, S. Fujita, *Jpn. J. Appl. Phys.* **2009**, *48*, 070202.

[66] T. Oshima, T. Okuno, *Jpn. J. Appl. Phys.* **2007**, *46*, 7217.

[67] J. Vlček, D. Kolenatý, J. Houška, T. Kozák, R. Čerstvý, *J. Phys. D* **2017**, *50*, 38LT01.

[68] X. Du, W. Mi, C. Luan, Z. Li, C. Xia, J. Ma, *J. Cryst. Growth* **2014**, *404*, 75.

[69] M. Becker, A. Polity, P. J. Klar, B. K. Meyer, *Phys. Status Solidi RRL* **2015**, *9*, 326.

[70] B. Eifert, M. Becker, C. T. Reindl, M. Giar, L. Zheng, A. Polity, Y. He, C. Heiliger, P. J. Klar, *Phys. Rev. Mat.* **2017**, *1*, 014602.

[71] T. Sander, C. T. Reindl, M. Giar, B. Eifert, M. Heinemann, C. Heiliger, P. J. Klar, *Phys. Rev. B* **2014**, *90*, 045203.

[72] D. B. Williams, C. B. Carter, Transmission Electron Microscopy, Sprinter-Verlag, New York **2009**.

[73] D. Severin, O. Kappertz, T. Nyberg, S. Berg, M. Wuttig, *Thin Solid Films* **2007**, *515*, 3554.

[74] D. Shinohara, S. Fujita, *Jpn. J. Appl. Phys.* **2008**, *47*, 7311.

[75] Y. Yao, S. Okur, L. A. M. Lyle, G. S. Tompa, T. Salagaj, N. Sbrockey, R. F. Davis, L. M. Porter, *Mater. Res. Lett.* **2018**, *6*, 268.

[76] M. Kracht, A. Karg, M. Feneberg, J. Bläsing, J. Schörmann, R. Goldhahn, M. Eickhoff, *Phys. Rev. Appl.* **2018**, *10*, 024047.

[77] R. Schewski, G. Wagner, M. Baldini, D. Gogova, Z. Galazka, T. Schulz, T. Remmele, T. Markurt, H. von Wenckstern, M. Grundmann, O. Bierwagen, P. Vogt, M. Albrecht, *Appl. Phys. Express* **2015**, *8*, 011101.

[78] C. Kranert, C. Sturm, R. Schmidt-Grund, M. Grundmann, *Sci. Rep.* **2016**, *6*, 35964.